Mapping the cell-surface proteome underlying hippocampal mossy fiber synapse identity

Nuno Apóstolo[1,2], Samuel N. Smukowski[3], Jeroen Vanderlinden[1,2], Giuseppe Condomitti[1,2], Vasily Rybakin[4], Jolijn ten Bos[1,2], Sybren Portegies[1,2], Kristel M. Vennekens[1,2], Natalia V. Gounko[1,2,5], Keimpe D. Wierda[1,2], Jeffrey N. Savas[3,*], Joris de Wit[1,2,*]

Affiliations:

[1] VIB Center for Brain & Disease Research, Herestraat 49, 300 Leuven, Belgium

[2] KU Leuven, Department of Neurosciences, Leuven Brain Institute, Herestraat 49, 3000 Leuven, Belgium

[3] Department of Neurology, Northwestern University Feinberg School of Medicine, Chicago, IL 60611, USA

[4] Immunobiology, REGA Institute, Department of Microbiology and Immunology, KU Leuven, Leuven, Belgium

[5] Electron Microscopy Platform & VIB BioImaging Core, Herestraat 49, 3000 Leuven, Belgium

[*]Correspondence to: jeffrey.savas@northwestern.edu; joris.dewit@kuleuven.vib.be

Abstract:

Synaptic diversity is a key feature of neural circuits. Its underlying molecular basis is largely unknown, due to the challenge of analyzing the protein composition of specific synapse types. Here, we isolate the hippocampal mossy fiber (MF) synapse, taking advantage of its unique size and architecture, and dissect its proteome. We identify a rich cell-surface repertoire that includes adhesion proteins, guidance cue receptors, extracellular matrix (ECM) proteins, and proteins of unknown function. Among the latter, we find IgSF8, a previously uncharacterized neuronal receptor, and uncover its role in regulating MF synapse architecture and feedforward inhibition on CA3 pyramidal neurons. Our findings reveal a diverse MF synapse surface proteome and highlight the role of neuronal surface-ECM interactions in the specification of synapse identity and circuit formation.

One Sentence Summary:

Proteomic dissection of a specific synapse

Main Text:

Neural circuits are composed of distinct neuronal cell types connected in highly specific patterns. Establishing these patterns of connectivity critically relies on cell-surface proteins (CSPs) expressed in cell type-specific combinations. CSPs, including transmembrane, membrane-anchored, and secreted proteins, engage in networks of interactions that control neurite guidance, target selection, and synapse development required for the formation of functional circuits (*1*). Single-cell RNA sequencing has enabled the characterization of cell type-specific CSP repertoires (*2–6*), but determining how these dictate complex patterns of connectivity (*7*, *8*) poses a major challenge.

This challenge is exemplified by pyramidal neurons, which receive different types of synapses on their dendritic arbor, each with a distinct architecture, subcellular location, and functional properties. This synaptic diversity is essential for information processing in pyramidal neurons (*9*). Recent studies reveal a synapse type-specific localization and function of postsynaptic adhesion molecules in hippocampal pyramidal neuron dendrites (*10–12*), suggesting that compartmentalized distributions of CSPs contribute to the specification of synaptic structure and function. Analogous to single-cell sequencing, probing the mechanisms underlying synaptic diversity requires dissecting the molecular composition of specific synapse types. This has remained challenging, as microdissection or chemical labeling strategies combined with mass spectrometry (MS) (*13–15*) average different synapse types, and affinity purification of synapse type-specific protein complexes (*16*) requires genetically engineered mice. Here, we isolate the hippocampal mossy fiber (MF) synapse, a large and morphologically complex excitatory synapse (*17*) connecting dentate granule cell axons (mossy fibers) and CA3 pyramidal neuron dendrites in stratum lucidum (SL) (Fig. 1A, B), from wild-type (WT) tissue and map its CSP landscape.

To isolate a specific synapse type from the hippocampus, we started with a previously published approach (*18*) that takes advantage of the MF-CA3 synapse's large size. We verified that this method enriches for MF-CA3 synaptosomes (fig. S1) and subsequently adapted the procedure to increase efficiency and improve enrichment of synaptic material (Fig. 1C). We accelerated the procedure by omitting gradient centrifugation and depleting myelin from the sample (fig. S2A). To improve enrichment of synaptic material, we utilized a fluorescence-activated synaptosome sorting (*19*) approach in which we labeled MF-CA3 synaptosomes with a fluorophore-conjugated monoclonal antibody against the extracellular domain of Nectin-3 (fig. S2B), a CA3-expressed adhesion protein that localizes to puncta adherentia junctions in mature MF-CA3 synapses (*20*), and FM4-64 membrane dye (fig. S2C, D). Western blot (WB) analysis of sorted MF-CA3 synaptosomes revealed a robust enrichment of MF-CA3 synapse markers Synaptoporin (Synpr) and Nectin-3, and depletion of myelin and nuclear markers (fig. S2E). Immunofluorescence analysis confirmed the presence of Synpr-, Nectin-3-, and vesicular glutamate transporter 1 (VGluT1)-positive large synaptosomes and depletion of Hoechst-positive nuclei in the sorted sample (fig. S2F and G), demonstrating feasibility of our approach to isolate MF-CA3 synaptosomes from hippocampal tissue.

To dissect the MF-CA3 synapse proteome, we compared fluorescently sorted MF-CA3 synaptosomes to P2 synaptosomes isolated in parallel from the same homogenate (fig. S2A). P2 synaptosomes represent a mixed population of small hippocampal synapses and serve as a background reference in our analysis. We analyzed sorted MF-CA3 synaptosomes and P2 synaptosomes from three independent experiments (10-12 mice per experiment) by LC-MS/MS. We identified 3592 proteins with at least 3 peptide identifications among replicates, and 11,6% and 7,9% of these proteins were exclusive to sorted MF-CA3 synaptosomes or P2 synaptosomes,

respectively (Fig. 1D and table S1). Gene ontology (GO) analysis showed a similar enrichment for synaptic terms in sorted MF-CA3 and P2 synaptosomes (fig. S3A). We calculated $\log_2$ fold-change (FC) enrichment in sorted MF-CA3 versus P2 synaptosomes using a label-free semi-quantitative approach based on the normalized spectral abundance factor (NSAF) (Fig. 1E; fig. S3B and table S1). Our analysis revealed 605 significant proteins with positive MF-CA3/P2 FC, and 138 significant proteins exclusively detected in sorted MF-CA3 synaptosomes (Fig. 1E; table S1). This MF-CA3 synaptic proteome (fig. S3C) comprises multiple proteins previously reported to be strongly enriched at MF-CA3 synapses, including the synaptic vesicle-associated proteins Synpr, Syn3, Rabphilin-3A, and ZnT3; the glutamate receptors GluK2 and mGluR3; the presynaptic scaffold protein liprin-α2; the dense core vesicle secretion-related protein CAPS2; and the puncta adherentia junction-associated proteins Nectin-3 and Af-6 (Fig. 1E; fig. S3D). We confirmed Syn3, Af-6, mGluR2/3, and ZnT3 localization to SL using immunohistochemistry (IHC) (Fig. 1F). These validations indicate that our approach confidently identifies MF-CA3 synaptic proteins.

Using the UniProt database to query our results for transmembrane, membrane-anchored, and secreted proteins among the MF-CA3 synaptic proteome, we identified a rich repertoire of CSPs that includes adhesion proteins, receptors, secreted glycoproteins, receptor protein tyrosine phosphatases and tyrosine kinases (Fig. 2A and table S2). Most major CSP protein families, such as the immunoglobulin (Ig) superfamily (IgSF), fibronectin type-III (FN3), and leucine-rich repeat (LRR) family, are represented (Fig. 2B). Only a small proportion (20,8%) of these CSPs has previously been reported to localize or function at MF-CA3 synapses (table S2). Using the synapse biology GO database SynGO (*21*), we determined that 48% of the identified CSPs genes lack a SynGO annotation (Fig. 2C), suggesting that these are novel candidate synaptic CSPs. The

secreted protein BRINP2 and the receptors FAM171A2, APMAP, and IgSF8 lack a function in the brain altogether (Fig. 2C).

To validate these findings, we tested a large panel of antibodies for detection of CSPs by WB and IHC (table S2). We validated the presence of 15 CSPs in sorted MF-CA3 synaptosomes by WB, including BRINP2 and IgSF8 (Fig. 2D). Using IHC on postnatal day (P) 28 mouse hippocampal sections, we confirmed localization to the MF-CA3 pathway for 21 CSPs (Fig. 2E; fig. S4). Of the CSPs lacking synaptic function, the axon guidance-related receptors ISLR2, Neogenin 1, ROBO2, Plexin-A3, and secreted protein CRTAC1 (*22*), displayed strongly enriched immunoreactivity in SL (Fig. 2E). We further confirmed robust localization to SL of the GPI-anchored protein Negr1 (Fig. 2E). Of the CSPs without a known function in the brain, we validated the presence of FAM171A2 in SL and observed strong labeling for IgSF8 in the MF-CA3 pathway (Fig. 2E). Together, these results confirm the presence of a diverse repertoire of CSPs at MF-CA3 synapses.

IgSF8 was of particular interest due to its strong localization to the MF-CA3 tract (Fig. 2E) and lack of known brain function. IgSF8 (Fig. 3A) has previously been detected in excitatory postsynaptic densities (PSDs) (*14*) and active zone (AZ) membrane preparations (*23*), but not in synaptic cleft proteomes (*24*, *25*). IgSF8 is highly expressed in the nervous system (*26*) and localizes to axons and presynaptic terminals of olfactory sensory neurons during synaptogenesis (*27*). We analyzed IgSF8 expression in hippocampal lysates and found that IgSF8 protein levels mildly increased during postnatal development (fig. S5A). To determine the synaptic localization of IgSF8, we performed subcellular fractionation, as the conditions required for IgSF8 IHC proved unsuitable for high-resolution imaging. IgSF8 mainly distributed to the Triton-soluble fraction of

synaptosomes containing the presynaptic protein Synaptophysin (fig. S5B), supporting a presynaptic localization.

As a presynaptic receptor, IgSF8 might interact with other synaptic CSPs. To identify synaptic ligands for IgSF8, we performed affinity chromatography using recombinant IgSF8-ecto-Fc as bait on whole brain synaptosome extract (fig. S6A and table S3) and MF-CA3 synaptosome extract (fig. S6B and table S3) and analyzed bound proteins by LC-MS/MS. We identified Tenascin-R (TenR), an ECM protein with roles in cell adhesion, synaptic transmission and plasticity (*28*), as the main IgSF8 binding partner in both experiments. We validated the IgSF8-TenR interaction using cell-surface binding assays and pull-down assays in HEK293T cells (fig. S6C and D). To test whether IgSF8 and TenR interact directly, we mixed equimolar amounts of Fc control protein, TenR-Fc, or Brevican-Fc, another brain ECM protein, with His-IgSF8 recombinant protein and precipitated Fc proteins. We found that the IgSF8-TenR interaction is direct and specific (fig. S6E). TenR is among the CSPs we identified in the MF-CA3 synapse proteome (Fig. 2C and table S2), indicating that our approach is capable of isolating both receptor and ligand at MF-CA3 synapses.

To determine the functional significance of IgSF8 for MF-CA3 synapse development, we removed IgSF8 presynaptically by crossing *Igsf8* conditional knockout (cKO) mice with the dentate granule cell-specific Rbp4-Cre line. This selectively abolished IgSF8 immunoreactivity in CA3 SL, without affecting gross MF-CA3 tract morphology (Fig. 3B). Infecting cultured *Igsf8* cKO hippocampal neurons with a lentiviral (LV) vector harboring Cre recombinase robustly reduced IgSF8 protein levels (fig. S7), validating the utility of the *Igsf8* cKO line for assessing IgSF8 function. We prepared hippocampal sections from P30 *Rbp4-Cre:Igsf8* cKO and control littermates and imaged MF-CA3 synapses by transmission electron microscopy (TEM) (Fig. 3C).

Bouton number and area were not affected in *Igsf8* cKO (fig. S8A and B), but we observed a clear reduction in AZ number and length, and a corresponding decrease in PSD number and length (Fig. 3D). To analyze MF bouton morphology, we injected adeno-associated viral (AAV) vectors expressing membrane-GFP (mGFP) and Cre recombinase in *Igsf8* cKO mice to remove IgSF8 expression (Fig. 3E). AAV-mGFP was used as a control. We observed a mild reduction in MF bouton volume, but a dramatic decrease in the number of filopodia emerging from the main bouton in *Igsf8* cKO (Fig. 3F and G). These results indicate that IgSF8 plays a role in shaping MF-CA3 synapse architecture and morphology.

To analyze functional changes at MF-CA3 synapses in the absence of IgSF8, we performed whole-cell voltage-clamp recordings of CA3 neurons in acute hippocampal slices from P27-35 *Rbp4-Cre:Igsf8* cKO and control littermates. Frequency and amplitude of spontaneous excitatory postsynaptic currents (sEPSCs) were reduced in *Igsf8* cKO mice (Fig. 4A to E), whereas decay time was not affected (fig. S9A). Histogram analysis showed a loss of large-amplitude sEPSCs (fig. S9B and C), which originate from MF-CA3 synapses (*29*), consistent with the decrease in number and length of synaptic junctions observed in *Igsf8* cKO mice. To specifically assess transmission at MF-CA3 synapses, we expressed Cre-dependent Channelrhodopsin-2 (DIO-ChR2) in *Rbp4-Cre:Igsf8* cKO and control littermates and optically stimulated MF axons while recording from CA3 neurons (Fig. 4F). We analyzed paired-pulse facilitation, a form of short-term plasticity, to assess MF-CA3 presynaptic properties, but found no differences in the amplitude of the first evoked EPSC or paired-pulse ratio between *Igsf8* cKO and control mice (fig. S9D to F), suggesting that evoked transmission at MF-CA3 synapses is not altered in the absence of IgSF8.

The filopodia emerging from MF boutons synapse onto interneurons in SL that mediate feedforward inhibition (FFI) on CA3 neurons (*30*, *31*). Given the dramatic decrease in the number

of filopodia in boutons of *Igsf8* cKO mice (Fig. 3F and G), we hypothesized that FFI would be reduced. Indeed, we observed a robust increase in the excitation-inhibition ratio when measuring light-evoked EPSCs and IPSCs from the same CA3 neuron (Fig. 4G to I). To determine the consequences of reduced FFI, we optically stimulated MF axons with a 10 Hz train of 20 stimuli and observed that CA3 neurons in *Igsf8* cKO mice fired action potentials earlier in the train than in controls (Fig. 4J to L), supporting the notion that reduced FFI in the absence of IgSF8 leads to increased excitability of CA3 neurons. Together, these results indicate that IgSF8 promotes MF bouton filopodia density to control microcircuit development and CA3 neuron excitability.

Our approach to isolate MF-CA3 synaptosomes and map their surface proteome provides the first insight into the CSP landscape of a specific excitatory synapse. We identify a rich CSP repertoire at MF-CA3 synapses. Our data suggest that multiple CSP complexes, likely acting in parallel, contribute to the specification of MF-CA3 synapse identity (fig. S10). The diverse CSP repertoire may also reflect heterogeneity among MF-CA3 synapses. MF synapse maturation varies due to the continuous integration of newborn granule cells into the hippocampal circuit (*32*), and distinct histories of synaptic activity may further diversify CSP composition. One of the CSPs without a previously characterized brain function we uncover at MF-CA3 synapses is the receptor IgSF8, which regulates synapse architecture, MF filopodia density, and FFI in the MF-CA3 microcircuit. The cytoplasmic tail of IgSF8 binds Ezrin-Radixin-Moesin (ERM) (*33*) and alpha-actinin (*34*), both of which are linked to filopodia formation. We identify the ECM protein TenR as a novel ligand of IgSF8. TenR induces actin-rich protrusions in cultured neurons (*35*), suggesting that the IgSF8-TenR interaction may promote formation or stabilization of MF filopodia. TenR is one of multiple ECM proteins in the MF-CA3 synaptic proteome, which also includes the largely uncharacterized ECM proteins Crtac1 and Brinp2 (*36*). ECM proteins play

important roles in the development of synaptic connectivity (*37*) but remain poorly understood. Our findings emphasize the role of neuronal surface-ECM interactions at MF-CA3 synapses (fig. S10).

The approach taken here may be applicable to other types of synapses. Our data can be used as a resource to explore other aspects of the MF-CA3 synapse, including molecular mechanisms of synaptic transmission, and may be of use in efforts to model synaptic connectivity in the dentate gyrus (*38*). Dissecting the molecular composition of specific synapse types will be an essential step toward molecular connectomics (*39*).

References and Notes:

1. J. de Wit, A. Ghosh, Specification of synaptic connectivity by cell surface interactions. *Nat. Rev. Neurosci.* **17**, 22–35 (2016).
2. C. Földy, S. Darmanis, J. Aoto, R. C. Malenka, S. R. Quake, T. C. Südhof, Single-cell RNAseq reveals cell adhesion molecule profiles in electrophysiologically defined neurons. *Proc. Natl. Acad. Sci. U.S.A.* **113**, E5222-5231 (2016).
3. H. Li, F. Horns, B. Wu, Q. Xie, J. Li, T. Li, D. J. Luginbuhl, S. R. Quake, L. Luo, Classifying Drosophila Olfactory Projection Neuron Subtypes by Single-Cell RNA Sequencing. *Cell*. **171**, 1206-1220.e22 (2017).
4. A. Paul, M. Crow, R. Raudales, M. He, J. Gillis, Z. J. Huang, Transcriptional Architecture of Synaptic Communication Delineates GABAergic Neuron Identity. *Cell*. **171**, 522-539.e20 (2017).
5. K. Shekhar, S. W. Lapan, I. E. Whitney, N. M. Tran, E. Z. Macosko, M. Kowalczyk, X. Adiconis, J. Z. Levin, J. Nemesh, M. Goldman, S. A. McCarroll, C. L. Cepko, A. Regev, J. R. Sanes, Comprehensive Classification of Retinal Bipolar Neurons by Single-Cell Transcriptomics. *Cell*. **166**, 1308-1323.e30 (2016).
6. E. Favuzzi, R. Deogracias, A. Marques-Smith, P. Maeso, J. Jezequel, D. Exposito-Alonso, M. Balia, T. Kroon, A. J. Hinojosa, E. F Maraver, B. Rico, Distinct molecular programs regulate synapse specificity in cortical inhibitory circuits. *Science*. **363**, 413–417 (2019).
7. K. Shen, P. Scheiffele, Genetics and cell biology of building specific synaptic connectivity. *Annu. Rev. Neurosci.* **33**, 473–507 (2010).
8. J. R. Sanes, M. Yamagata, Many paths to synaptic specificity. *Annu. Rev. Cell Dev. Biol.* **25**, 161–195 (2009).
9. N. Spruston, Pyramidal neurons: dendritic structure and synaptic integration. *Nat. Rev. Neurosci.* **9**, 206–221 (2008).
10. R. Sando, X. Jiang, T. C. Südhof, Latrophilin GPCRs direct synapse specificity by coincident binding of FLRTs and teneurins. *Science*. **363** (2019), doi:10.1126/science.aav7969.
11. A. Schroeder, J. Vanderlinden, K. Vints, L. F. Ribeiro, K. M. Vennekens, N. V. Gounko, K. D. Wierda, J. de Wit, A Modular Organization of LRR Protein-Mediated Synaptic Adhesion Defines Synapse Identity. *Neuron*. **99**, 329-344.e7 (2018).
12. G. Condomitti, K. D. Wierda, A. Schroeder, S. E. Rubio, K. M. Vennekens, C. Orlandi, K. A. Martemyanov, N. V. Gounko, J. N. Savas, J. de Wit, An Input-Specific Orphan Receptor GPR158-HSPG Interaction Organizes Hippocampal Mossy Fiber-CA3 Synapses. *Neuron*. **100**, 201-215.e9 (2018).
13. K. Sharma, S. Schmitt, C. G. Bergner, S. Tyanova, N. Kannaiyan, N. Manrique-Hoyos, K. Kongi, L. Cantuti, U.-K. Hanisch, M.-A. Philips, M. J. Rossner, M. Mann, M. Simons, Cell type- and brain region-resolved mouse brain proteome. *Nat. Neurosci.* **18**, 1819–1831 (2015).
14. A. Uezu, D. J. Kanak, T. W. A. Bradshaw, E. J. Soderblom, C. M. Catavero, A. C. Burette, R. J. Weinberg, S. H. Soderling, Identification of an elaborate complex mediating postsynaptic inhibition. *Science*. **353**, 1123–1129 (2016).
15. M. Roy, O. Sorokina, C. McLean, S. Tapia-González, J. DeFelipe, J. D. Armstrong, S. G. N. Grant, Regional Diversity in the Postsynaptic Proteome of the Mouse Brain. *Proteomes*. **6** (2018), doi:10.3390/proteomes6030031.
16. F. Selimi, I. M. Cristea, E. Heller, B. T. Chait, N. Heintz, Proteomic studies of a single CNS synapse type: the parallel fiber/purkinje cell synapse. *PLoS Biol.* **7**, e83 (2009).
17. R. A. Nicoll, D. Schmitz, Synaptic plasticity at hippocampal mossy fibre synapses. *Nat. Rev. Neurosci.* **6**, 863–876 (2005).
18. P. Taupin, S. Zini, F. Cesselin, Y. Ben-Ari, M. P. Roisin, Subcellular fractionation on Percoll gradient of mossy fiber synaptosomes: morphological and biochemical characterization in control and degranulated rat hippocampus. *J. Neurochem.* **62**, 1586–1595 (1994).
19. C. Biesemann, M. Grønborg, E. Luquet, S. P. Wichert, V. Bernard, S. R. Bungers, B. Cooper, F. Varoqueaux, L. Li, J. A. Byrne, H. Urlaub, O. Jahn, N. Brose, E. Herzog, Proteomic screening of glutamatergic mouse brain synaptosomes isolated by fluorescence activated sorting. *EMBO J.* **33**, 157–170 (2014).
20. A. Mizoguchi, H. Nakanishi, K. Kimura, K. Matsubara, K. Ozaki-Kuroda, T. Katata, T. Honda, Y. Kiyohara, K. Heo, M. Higashi, T. Tsutsumi, S. Sonoda, C. Ide, Y. Takai, Nectin: an adhesion molecule involved in formation of synapses. *J. Cell Biol.* **156**, 555–565 (2002).
21. F. Koopmans, P. van Nierop, M. Andres-Alonso, A. Byrnes, T. Cijsouw, M. P. Coba, L. N. Cornelisse, R. J. Farrell, H. L. Goldschmidt, D. P. Howrigan, N. K. Hussain, C. Imig, A. P. H. de Jong, H. Jung, M. Kohansalnodehi, B. Kramarz, N. Lipstein, R. C. Lovering, H. MacGillavry, V. Mariano, H. Mi, M. Ninov, D.

Osumi-Sutherland, R. Pielot, K.-H. Smalla, H. Tang, K. Tashman, R. F. G. Toonen, C. Verpelli, R. Reig-Viader, K. Watanabe, J. van Weering, T. Achsel, G. Ashrafi, N. Asi, T. C. Brown, P. De Camilli, M. Feuermann, R. E. Foulger, P. Gaudet, A. Joglekar, A. Kanellopoulos, R. Malenka, R. A. Nicoll, C. Pulido, J. de Juan-Sanz, M. Sheng, T. C. Südhof, H. U. Tilgner, C. Bagni, À. Bayés, T. Biederer, N. Brose, J. J. E. Chua, D. C. Dieterich, E. D. Gundelfinger, C. Hoogenraad, R. L. Huganir, R. Jahn, P. S. Kaeser, E. Kim, M. R. Kreutz, P. S. McPherson, B. M. Neale, V. O'Connor, D. Posthuma, T. A. Ryan, C. Sala, G. Feng, S. E. Hyman, P. D. Thomas, A. B. Smit, M. Verhage, SynGO: An Evidence-Based, Expert-Curated Knowledge Base for the Synapse. *Neuron*. **103**, 217-234.e4 (2019).

22. Y. Sato, M. Iketani, Y. Kurihara, M. Yamaguchi, N. Yamashita, F. Nakamura, Y. Arie, T. Kawasaki, T. Hirata, T. Abe, H. Kiyonari, S. M. Strittmatter, Y. Goshima, K. Takei, Cartilage acidic protein-1B (LOTUS), an endogenous Nogo receptor antagonist for axon tract formation. *Science*. **333**, 769–773 (2011).

23. J. Weingarten, M. Lassek, B. F. Mueller, M. Rohmer, I. Lunger, D. Baeumlisberger, S. Dudek, P. Gogesch, M. Karas, W. Volknandt, The proteome of the presynaptic active zone from mouse brain. *Mol. Cell. Neurosci.* **59**, 106–118 (2014).

24. K. H. Loh, P. S. Stawski, A. S. Draycott, N. D. Udeshi, E. K. Lehrman, D. K. Wilton, T. Svinkina, T. J. Deerinck, M. H. Ellisman, B. Stevens, S. A. Carr, A. Y. Ting, Proteomic Analysis of Unbounded Cellular Compartments: Synaptic Clefts. *Cell*. **166**, 1295-1307.e21 (2016).

25. T. Cijsouw, A. M. Ramsey, T. T. Lam, B. E. Carbone, T. A. Blanpied, T. Biederer, Mapping the Proteome of the Synaptic Cleft through Proximity Labeling Reveals New Cleft Proteins. *Proteomes*. **6** (2018), doi:10.3390/proteomes6040048.

26. J. N. Murdoch, K. Doudney, D. Gerrelli, N. Wortham, C. Paternotte, P. Stanier, A. J. Copp, Genomic organization and embryonic expression of Igsf8, an immunoglobulin superfamily member implicated in development of the nervous system and organ epithelia. *Mol. Cell. Neurosci.* **22**, 62–74 (2003).

27. A. Ray, H. B. Treloar, IgSF8: a developmentally and functionally regulated cell adhesion molecule in olfactory sensory neuron axons and synapses. *Mol. Cell. Neurosci.* **50**, 238–249 (2012).

28. A. Dityatev, M. Schachner, P. Sonderegger, The dual role of the extracellular matrix in synaptic plasticity and homeostasis. *Nat. Rev. Neurosci.* **11**, 735–746 (2010).

29. D. A. Henze, D. B. T. McMahon, K. M. Harris, G. Barrionuevo, Giant miniature EPSCs at the hippocampal mossy fiber to CA3 pyramidal cell synapse are monoquantal. *J. Neurophysiol.* **87**, 15–29 (2002).

30. N. Rebola, M. Carta, C. Mulle, Operation and plasticity of hippocampal CA3 circuits: implications for memory encoding. *Nat. Rev. Neurosci.* **18**, 208–220 (2017).

31. L. Acsády, A. Kamondi, A. Sík, T. Freund, G. Buzsáki, GABAergic cells are the major postsynaptic targets of mossy fibers in the rat hippocampus. *J. Neurosci.* **18**, 3386–3403 (1998).

32. N. Toni, D. A. Laplagne, C. Zhao, G. Lombardi, C. E. Ribak, F. H. Gage, A. F. Schinder, Neurons born in the adult dentate gyrus form functional synapses with target cells. *Nat. Neurosci.* **11**, 901–907 (2008).

33. M. Sala-Valdés, A. Ursa, S. Charrin, E. Rubinstein, M. E. Hemler, F. Sánchez-Madrid, M. Yáñez-Mó, EWI-2 and EWI-F link the tetraspanin web to the actin cytoskeleton through their direct association with ezrin-radixin-moesin proteins. *J. Biol. Chem.* **281**, 19665–19675 (2006).

34. M. Gordón-Alonso, M. Sala-Valdés, V. Rocha-Perugini, D. Pérez-Hernández, S. López-Martín, A. Ursa, S. Alvarez, T. V. Kolesnikova, J. Vázquez, F. Sánchez-Madrid, M. Yáñez-Mó, EWI-2 association with α-actinin regulates T cell immune synapses and HIV viral infection. *J. Immunol.* **189**, 689–700 (2012).

35. U. Zacharias, R. Leuschner, U. Nörenberg, F. G. Rathjen, Tenascin-R induces actin-rich microprocesses and branches along neurite shafts. *Mol. Cell. Neurosci.* **21**, 626–633 (2002).

36. S. R. Berkowicz, T. J. Featherby, J. C. Whisstock, P. I. Bird, Mice Lacking Brinp2 or Brinp3, or Both, Exhibit Behaviors Consistent with Neurodevelopmental Disorders. *Frontiers in Behavioral Neuroscience*. **10** (2016), doi:10.3389/fnbeh.2016.00196.

37. M. Yuzaki, Two Classes of Secreted Synaptic Organizers in the Central Nervous System. *Annu. Rev. Physiol.* **80**, 243–262 (2018).

38. P. Jonas, J. Lisman, Structure, function, and plasticity of hippocampal dentate gyrus microcircuits. *Front Neural Circuits*. **8**, 107 (2014).

39. D. Schreiner, J. N. Savas, E. Herzog, N. Brose, J. de Wit, Synapse biology in the 'circuit-age'-paths toward molecular connectomics. *Curr. Opin. Neurobiol.* **42**, 102–110 (2017).

40. J. de Wit, E. Sylwestrak, M. L. O'Sullivan, S. Otto, K. Tiglio, J. N. Savas, J. R. Yates, D. Comoletti, P. Taylor, A. Ghosh, LRRTM2 interacts with Neurexin1 and regulates excitatory synapse formation. *Neuron*. **64**, 799–806 (2009).

41. N. Inoue, T. Nishikawa, M. Ikawa, M. Okabe, Tetraspanin-interacting protein IGSF8 is dispensable for mouse fertility. *Fertil. Steril.* **98**, 465–470 (2012).

42. L. F. Ribeiro, B. Verpoort, J. Nys, K. M. Vennekens, K. D. Wierda, J. de Wit, SorCS1-mediated sorting in dendrites maintains neurexin axonal surface polarization required for synaptic function. *PLoS Biol.* **17**, e3000466 (2019).

43. J. Mattis, K. M. Tye, E. A. Ferenczi, C. Ramakrishnan, D. J. O'Shea, R. Prakash, L. A. Gunaydin, M. Hyun, L. E. Fenno, V. Gradinaru, O. Yizhar, K. Deisseroth, Principles for applying optogenetic tools derived from direct comparative analysis of microbial opsins. *Nat. Methods*. **9**, 159–172 (2011).

44. J. de Wit, M. L. O'Sullivan, J. N. Savas, G. Condomitti, M. C. Caccese, K. M. Vennekens, J. R. Yates, A. Ghosh, Unbiased discovery of glypican as a receptor for LRRTM4 in regulating excitatory synapse development. *Neuron*. **79**, 696–711 (2013).

45. J. N. Savas, J. De Wit, D. Comoletti, R. Zemla, A. Ghosh, J. R. Yates, Ecto-Fc MS identifies ligand-receptor interactions through extracellular domain Fc fusion protein baits and shotgun proteomic analysis. *Nat Protoc*. **9**, 2061–2074 (2014).

46. L. He, J. Diedrich, Y.-Y. Chu, J. R. Yates, Extracting Accurate Precursor Information for Tandem Mass Spectra by RawConverter. *Anal. Chem.* **87**, 11361–11367 (2015).

47. J. K. Eng, A. L. McCormack, J. R. Yates, An approach to correlate tandem mass spectral data of peptides with amino acid sequences in a protein database. *J. Am. Soc. Mass Spectrom.* **5**, 976–989 (1994).

48. T. Xu, S. K. Park, J. D. Venable, J. A. Wohlschlegel, J. K. Diedrich, D. Cociorva, B. Lu, L. Liao, J. Hewel, X. Han, C. C. L. Wong, B. Fonslow, C. Delahunty, Y. Gao, H. Shah, J. R. Yates, ProLuCID: An improved SEQUEST-like algorithm with enhanced sensitivity and specificity. *J Proteomics*. **129**, 16–24 (2015).

49. D. L. Tabb, W. H. McDonald, J. R. Yates, DTASelect and Contrast: tools for assembling and comparing protein identifications from shotgun proteomics. *J. Proteome Res.* **1**, 21–26 (2002).

50. D. Cociorva, D. L Tabb, J. R. Yates, *Curr Protoc Bioinformatics*, in press, doi:10.1002/0471250953.bi1304s16.

51. L. Florens, M. J. Carozza, S. K. Swanson, M. Fournier, M. K. Coleman, J. L. Workman, M. P. Washburn, Analyzing chromatin remodeling complexes using shotgun proteomics and normalized spectral abundance factors. *Methods*. **40**, 303–311 (2006).

52. B. Zybailov, A. L. Mosley, M. E. Sardiu, M. K. Coleman, L. Florens, M. P. Washburn, Statistical analysis of membrane proteome expression changes in Saccharomyces cerevisiae. *J. Proteome Res.* **5**, 2339–2347 (2006).

53. H. Mi, A. Muruganujan, X. Huang, D. Ebert, C. Mills, X. Guo, P. D. Thomas, Protocol Update for large-scale genome and gene function analysis with the PANTHER classification system (v.14.0). *Nat Protoc*. **14**, 703–721 (2019).

54. R. K. Carlin, D. J. Grab, R. S. Cohen, P. Siekevitz, Isolation and characterization of postsynaptic densities from various brain regions: enrichment of different types of postsynaptic densities. *J. Cell Biol.* **86**, 831–845 (1980).

55. J. Schindelin, I. Arganda-Carreras, E. Frise, V. Kaynig, M. Longair, T. Pietzsch, S. Preibisch, C. Rueden, S. Saalfeld, B. Schmid, J.-Y. Tinevez, D. J. White, V. Hartenstein, K. Eliceiri, P. Tomancak, A. Cardona, Fiji: an open-source platform for biological-image analysis. *Nat. Methods*. **9**, 676–682 (2012).

56. I. Galimberti, N. Gogolla, S. Alberi, A. F. Santos, D. Muller, P. Caroni, Long-term rearrangements of hippocampal mossy fiber terminal connectivity in the adult regulated by experience. *Neuron*. **50**, 749–763 (2006).

Acknowledgments:

We thank Franck Polleux, Dietmar Schmucker, Pierre Vanderhaeghen, Dan Dascenco, Luís Ribeiro, and Sara Calafate for critical reading of the manuscript and De Wit lab members for discussion and comments. We thank Pier Andrée Penttila and Christèle Nkama (VIB-KU Leuven FACS Core), the VIB-KU Leuven BioImaging Core, and Joris Vandenbempt for experimental help; Nicola Fattorelli for data visualization advice; Etienne Herzog and Matthew Holt for experimental advice. **Funding:** Leica SP8x confocal microscope provided by InfraMouse (KU Leuven-VIB) through a Hercules type 3 project (ZW09-03). N.A. is supported by the Fundação para a Ciência e a Tecnologia (FCT, grant number SFRH/BD/128869/2017). J.N.S. is supported by R01AG061787. J.d.W is supported by ERC Starting Grant (#311083), FWO Odysseus Grant, FWO Project grant G0C4518N, FWO EOS grant G0H2818N, and Methusalem grant of KU Leuven/Flemish Government. **Author contributions:** N.A., J.N.S., and J.d.W. conceived the study and designed experiments. N.A., S.N.S, J.V., G.C., V.R., J.t.B., S.P., K.M.V., N.V.G., and K.D.W. performed experiments and analyzed data. N.A. and J.d.W. wrote the paper with input from all authors. All authors contributed to and approved the final version. **Competing interests:** The authors declare no competing interests. **Data and materials availability:** MS raw files and search results can be accessed via Proteome Exchange at PXD013492.

Supplementary Materials:

Materials and Methods

Figures S1-S10

Tables S1-S4

Table legends S1 to S4

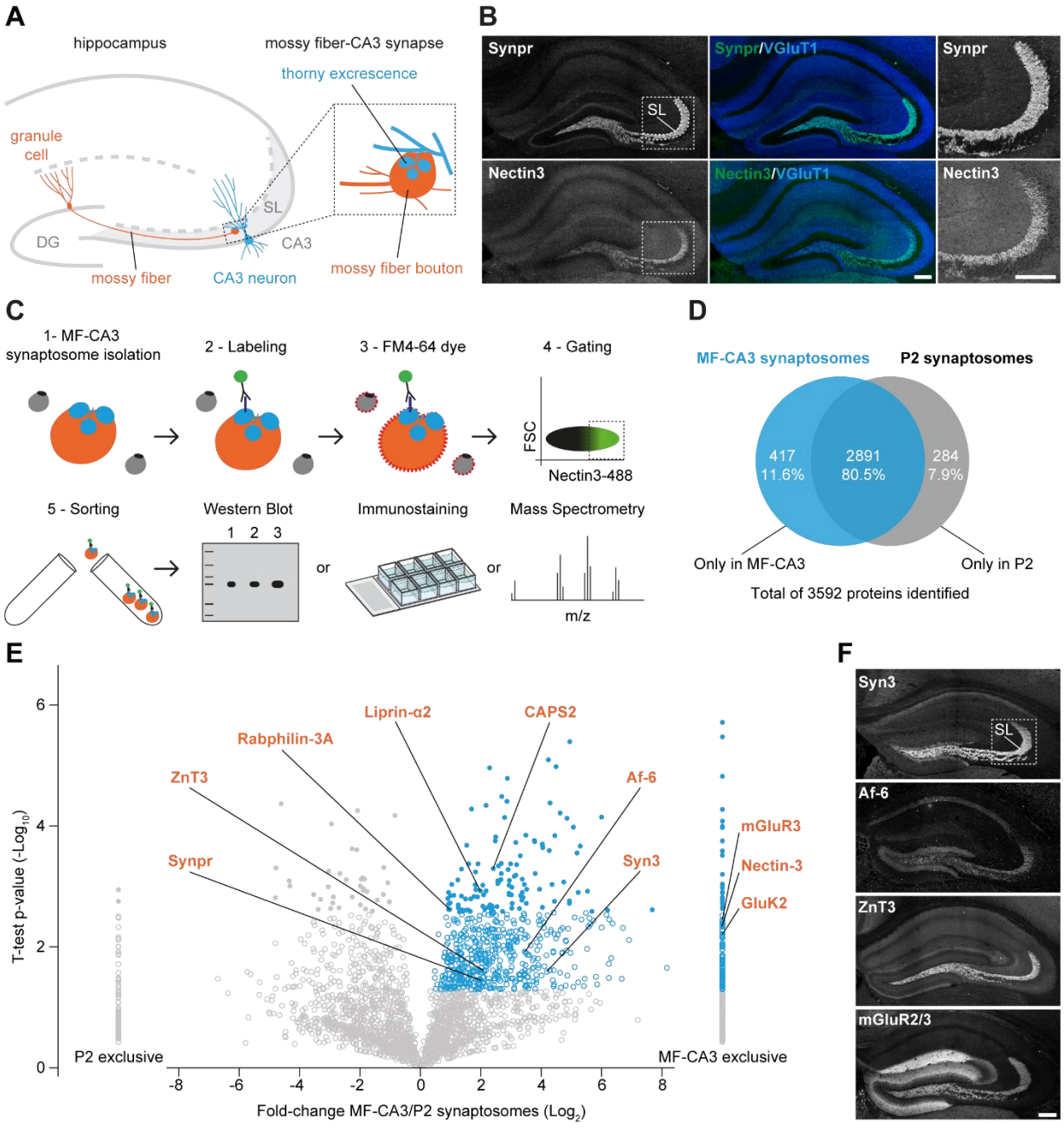

Fig. 1. Development of a strategy to analyze the MF-CA3 synaptic proteome. (**A**) Cartoon illustrating the large hippocampal MF-CA3 synapse. (**B**) Confocal images of P28 mouse hippocampal sections immunostained for Synpr, Nectin-3 and VGluT1. Magnified insets of the SL in CA3 are shown on the right. (**C**) Workflow to isolate and analyze MF-CA3 synaptosomes. (**D**) Venn diagram capturing number and distribution of proteins identified in sorted MF-CA3 synaptosomes and P2 synaptosomes by LC-MS/MS in three independent experiments (10-12 mice per experiment). (**E**) Relative distribution of proteins detected in sorted MF-CA3 synaptosomes and P2 synaptosomes. Significant proteins with positive MF-CA3/P2 $\log_2$ fold-change are highlighted in blue (p-value ≤ 0.05, Student's t-test). High-confidence measurements at a 5% FDR are shown as closed circles (q-value ≤ 0.05, Benjamini-Hochberg correction). A selection of

known MF-CA3 synaptic proteins is annotated in orange. (**F**) Confocal images of P28 mouse hippocampal sections immunostained for known MF-CA3 synaptic markers detected in the MF-CA3 synaptic proteome. Scale bars in (B) and (F) 200 μm.

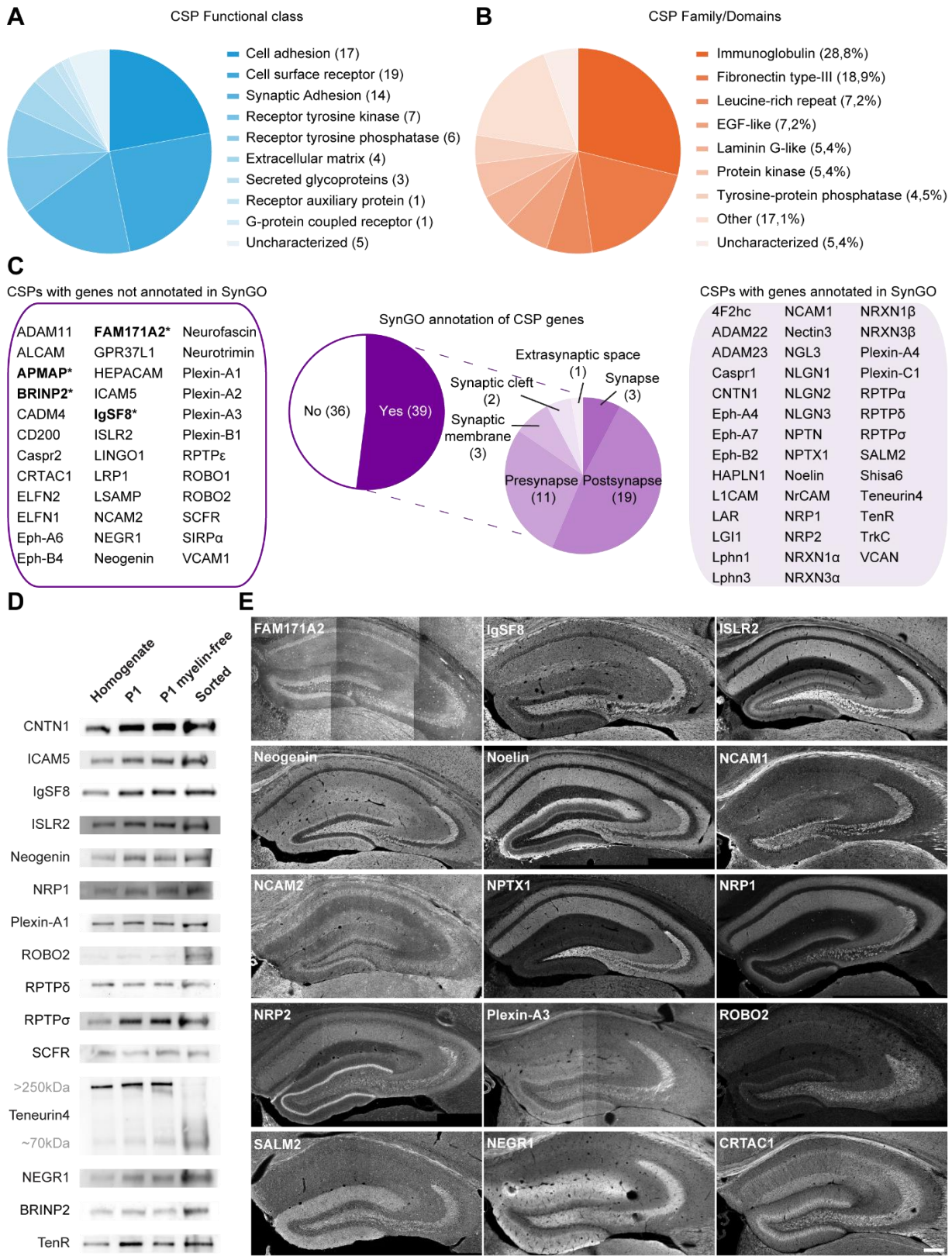

Fig. 2. Identification of CSPs expressed at MF-CA3 synapses. (**A**) Protein functional classes represented in the group of CSPs detected in the MF-CA3 synaptic proteome. (**B**) Occurrence of

protein domains among identified CSPs. (**C**) SynGO cellular component analysis of CSP genes (75) and respective CSPs (77). Proteins with unknown function in the brain are highlighted in bold with an asterisk. (**D**) Validation of a panel of CSPs in sorted MF-CA3 synaptosomes by western blot. (**E**) Confocal images of P28 mouse hippocampal sections immunostained for a panel of CSPs. Scale bar in (E) 200 μm.

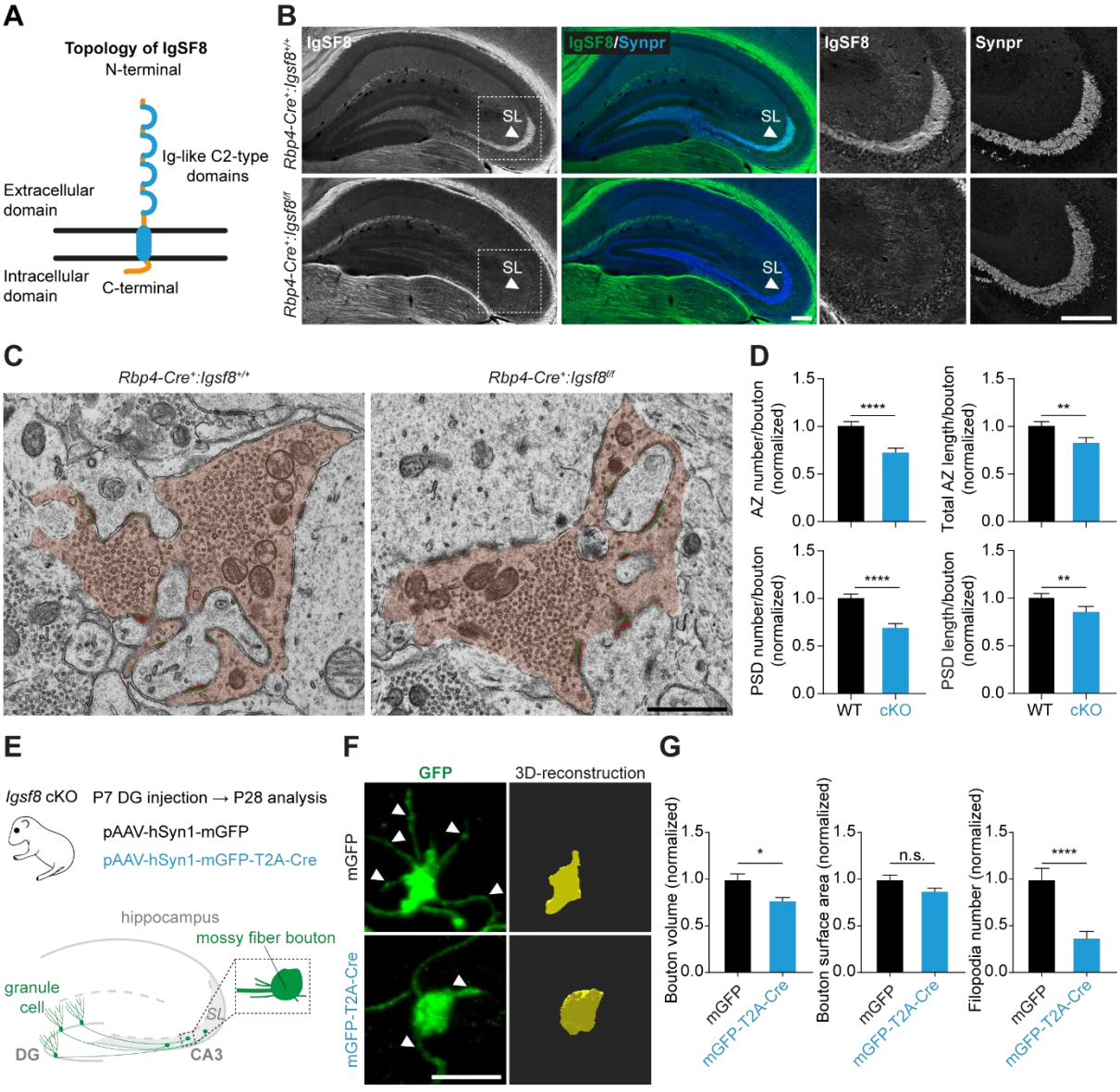

Fig. 3. Granule-cell specific deletion of IgSF8 alters MF-CA3 synaptic architecture. (**A**) Cartoon of IgSF8 protein topology. (**B**) Confocal images of P28 *Rbp4-Cre*:*Igsf8* cKO mouse hippocampal sections immunostained for IgSF8 and Synpr. Arrowheads indicate SL. Magnified insets of the SL in CA3 are shown on the right. (**C**) Electron microscope images of MF-CA3 synapses from *Rbp4-Cre*:*Igsf8* cKO and WT littermates (5000x magnification). MF boutons are highlighted in orange. AZs and PSDs are highlighted in green and red, respectively. (**D**) Graphs show quantification of analysis done in (C) using three littermate mice per condition (WT, n = 135 boutons; cKO, n = 136). (**E**) Experimental design to analyze structural changes in MF boutons following deletion of *Igsf8* specifically in DG granule cells. (**F**) Stacks of confocal images of individual MF boutons (left) and respective 3D reconstructions (right) to analyze MF bouton volume, surface area and number of filopodia. Arrowheads show filopodia emerging from MF boutons. (**G**) Graphs show quantification of analysis done in (F) using three littermate mice per condition (mGFP, n=27 boutons; mGFP-T2A-Cre n=29). Graphs show mean ± SEM. Mann-

Whitney tests were used. n.s., not significant; *$P < 0.05$; **$P < 0.01$; ****$P < 0.0001$. Scale bars in (B) 200 μm, in (C) 1 μm, and in (F) 5 μm.

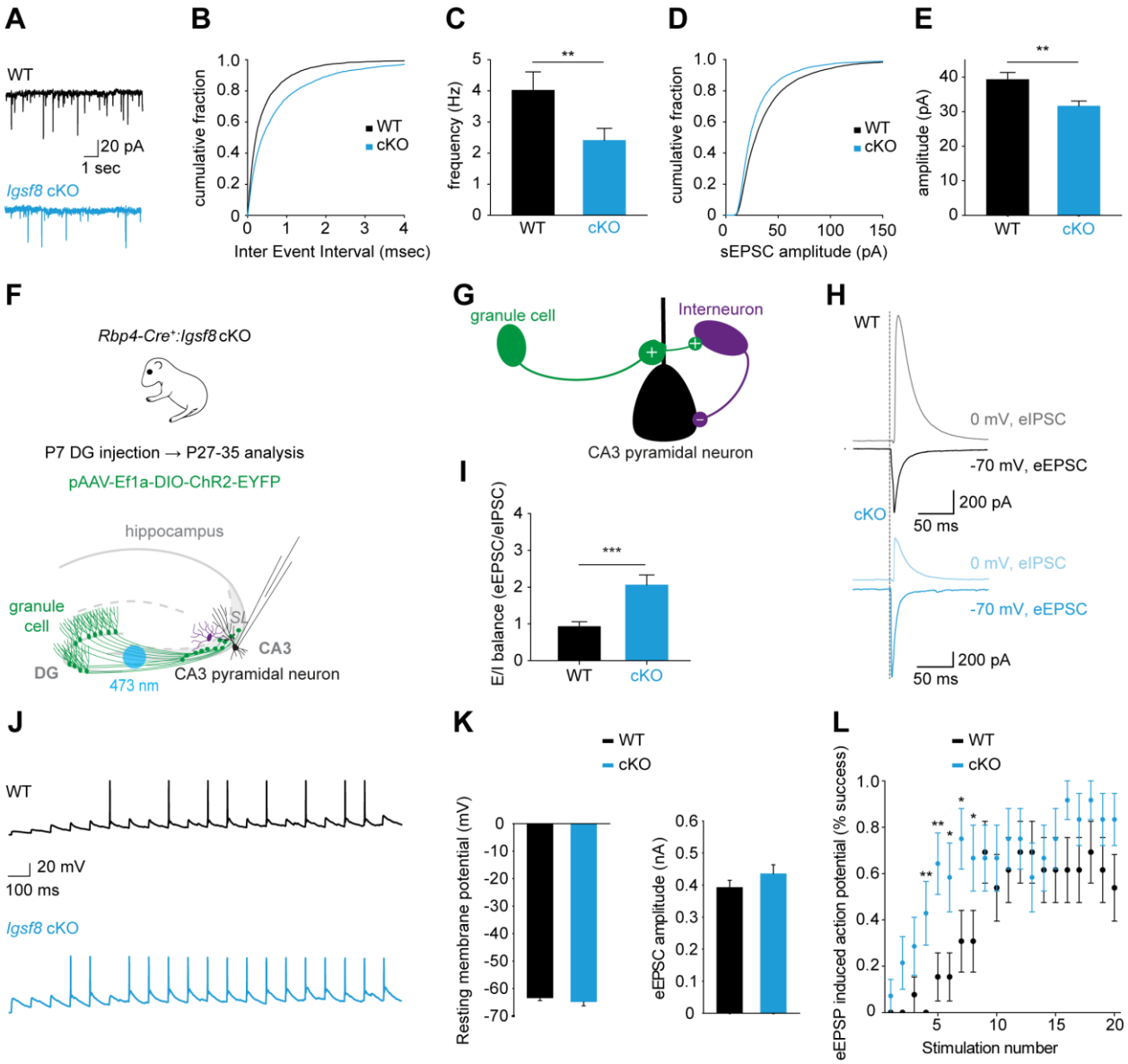

Fig. 4. IgSF8 controls feedforward inhibition in the CA3 microcircuit. (**A**) Representative sEPSC traces from whole-cell voltage-clamp recordings of CA3 neurons in acute hippocampal slices of *Rbp4-Cre*:*Igsf8* cKO and WT littermates. (**B**) Cumulative distribution of sEPSC inter-event intervals. (**C**) Quantification of sEPSC frequency. (**D**) Cumulative distribution of sEPSC amplitudes. (**E**) Quantification of sEPSC amplitudes. (**F**) Cartoon illustrating whole-cell voltage-clamp recordings of CA3 neurons to measure MF-evoked responses in acute hippocampal slices of *Rbp4-Cre*:*Igsf8* cKO and WT littermates using optogenetics. (**G**) Cartoon illustrating feedforward inhibition microcircuit in CA3. Plus and minus signs represent excitatory and inhibitory synapses, respectively. (**H**) Representative eEPSC and eIPSC traces from CA3 pyramidal neurons in WT or cKO mice. (**I**) Quantification of excitation-inhibition balance in CA3 neurons in WT and cKO mice. (**J**) Representative eEPSP traces from CA3 pyramidal neurons in WT or cKO mice. (**K**) Quantification of resting membrane potentials and eEPSC amplitudes of CA3 neurons in WT and cKO mice. (**L**) Quantification of induced action potential firing in CA3

neurons in WT and cKO mice after a 10 Hz train of 20 stimuli. Three littermate mice pairs were used per condition. For sEPSCs: WT, n = 31 neurons and cKO, n = 38. For eEPSCs and eIPSCs: WT, n = 35 neurons and cKO, n= 29. For eEPSPs: WT, n = 13 neurons and cKO, n= 14. Graphs show mean ± SEM. Mann-Whitney tests were used in (C), (E) and (I). Student's t-test was used in (L). n.s., not significant; $*P < 0.05$; $**P < 0.01$; $***P < 0.001$.